Review of CdTe$_{1-x}$Se$_x$ Thin Films in Solar Cell Applications

Martina Lingg * , **Stephan Buecheler and Ayodhya N. Tiwari**

Laboratory for Thin Films and Photovoltaics, Empa - Swiss Federal Laboratories for Materials Science and Technology, Ueberlandstrasse 129, 8600 Duebendorf, Switzerland
* Correspondence: martina.lingg@empa.ch

check for updates

Abstract: Recent improvements in CdTe thin film solar cells have been achieved by using CdTe$_{1-x}$Se$_x$ as a part of the absorber layer. This review summarizes the published literature concerning the material properties of CdTe$_{1-x}$Se$_x$ and its application in current thin film CdTe photovoltaics. One of the important properties of CdTe$_{1-x}$Se$_x$ is its band gap bowing, which facilitates a lowering of the CdTe band gap towards the optimum band gap for highest theoretical efficiency. In practice, a CdTe$_{1-x}$Se$_x$ gradient is introduced to the front of CdTe, which induces a band gap gradient and allows for the fabrication of solar cells with enhanced short-circuit current while maintaining a high open-circuit voltage. In some device structures, the addition of CdTe$_{1-x}$Se$_x$ also allows for a reduction in CdS thickness or its complete elimination, reducing parasitic absorption of low wavelength photons.

Keywords: CdTe; CdSe; CdTe$_{1-x}$Se$_x$; photovoltaics; solar cells; review

1. Introduction

With a global drive towards renewable energies, photovoltaics is an increasing part of global energy supply. CdTe is the leading technology amongst thin film solar cells for cost effective solar electricity production, due to its high photovoltaic conversion efficiency, long-term performance stability, low fabrication costs and short energy-payback time [1]. The current efficiency record for CdTe cells is 22.1%, held by First Solar [2,3].

In state-of-the-art CdTe solar cells, the J_{SC} is already close to its theoretical limit [4]. According to the Shockley–Queisser thermodynamic limit to solar cell efficiency, the optimum band gap for maximum theoretical solar cell efficiency under AM 1.5 G is 1.34 eV [5,6]; the band gap of CdTe is slightly too wide at 1.5 eV [4]. Strategies to shift the band gap of the CdTe absorber towards the theoretical optimum can help to further increase photocurrent and, consequently, the efficiency. CdTe$_{1-x}$Se$_x$ is a promising material for this purpose, as its band gap can be shifted down to 1.4 eV [7,8] by appropriately adjusting the composition. First Solar's world record cell efficiency was improved from 19.5% to 22.1% using an absorber with a lower band gap than CdTe, the CdTe$_{1-x}$Se$_x$ alloy [9–11].

With an absorber material that has an adjustable band gap, the band gap profile through the absorber layer can be engineered by applying a compositional grading. Different research groups have been investigating the use of a CdTe$_{1-x}$Se$_x$ layer towards the front of a CdTe absorber layer, resulting in champion devices with improved J_{SC} due to higher absorption in the low-band gap front layer, while maintaining the V$_{OC}$ from the bulk CdTe [8,12–17].

For traditional CdS/CdTe solar cells, a CdCl$_2$ treatment, generally consisting of deposition of CdCl$_2$ on the absorber and subsequent heating, is needed to recrystallize the absorber layer, resulting in increased CdTe grain size and intermixing of CdS and CdTe as well as modifications in electronic properties leading to enhancement in photovoltaic conversion efficiency [18]. If a CdSe or CdTe$_{1-x}$Se$_x$ layer is inserted in between CdS and CdTe, interdiffusion during CdCl$_2$ treatment results in a CdTe$_{1-x}$Se$_x$

layer. Because $CdTe_{1-x}Se_x$ has no miscibility gap, a continuous composition gradient is formed, with an associated band gap gradient [15,19], allowing for absorption of high-wavelength photons. Several research groups have also found that, with the use of a $CdTe_{1-x}Se_x$ front layer, the CdS window layer thickness can be reduced, or the CdS layer can even be omitted completely, reducing parasitic absorption in the short-wavelength region and further increasing J_{SC} [8,14,20]. A thick CdS layer is generally required to avoid direct contact between the transparent conducting oxide (TCO) and the CdTe absorber, but a $CdTe_{1-x}Se_x$ absorber seems to be less sensitive to this issue. Further improvement was achieved by replacing CdS with MgZnO, which has a more favorable band alignment with both CdTe and $CdTe_{1-x}Se_x$ than CdS, and which is more transparent in the short-wavelength region [15,21,22]. Additionally, passivation of defects due to Se has been reported to be responsible for the higher carrier lifetimes in $CdTe_{1-x}Se_x$ compared to CdTe [19,23].

CdTe technology has shifted in recent years from a traditional CdS/CdTe structure to a device structure that utilizes a $CdTe_{1-x}Se_x$ layer and a band gap gradient, but no CdS layer, in order to achieve high currents and voltages. In this review paper we discuss the steps of this transformation, from the first introduction of a $CdTe_{1-x}Se_x$ layer to the complete replacement of the CdS layer by MgZnO and $CdTe_{1-x}Se_x$. We discuss the material properties of $CdTe_{1-x}Se_x$ and their dependence on composition and the application of this material in thin-film solar cells.

2. Growth of $CdTe_{1-x}Se_x$ Thin Films and Material Properties

In this section, we will discuss the deposition of $CdTe_{1-x}Se_x$ films and their structural, optical and electronic properties.

$CdTe_{1-x}Se_x$ is a solid solution without a miscibility gap; the alloy is stable over the complete composition range $0 \leq x \leq 1$. Thin films of desired composition can be grown with a variety of methods, such as high-vacuum evaporation of the elements [24] or the alloy $CdTe_{1-x}Se_x$ [25,26], co-evaporation of CdTe and CdSe [8,27], close space sublimation of the alloy $CdTe_{1-x}Se_x$ [23,28] or co-sublimation of the components CdTe and CdSe [29], molecular beam epitaxy [30,31], hot wall deposition [32], electron beam deposition [7,33], or electrodeposition [34,35]. The properties of grown layers depend on the deposition method and the conditions used.

In solar cells, the main methods used for $CdTe_{1-x}Se_x$ formation are high-vacuum evaporation [8] or radio frequency sputtering [14,16,20] of a CdSe layer next to a CdTe layer, with interdiffusion during $CdCl_2$ treatment, or close space sublimation of a $CdTe_{1-x}Se_x$ layer next to a CdTe layer [15], which also interdiffuse during $CdCl_2$ treatment. Close space sublimation is performed at higher temperatures than high-vacuum deposition or sputtering, and in CdTe it results in very large grains. The lower deposition temperature of high-vacuum evaporation results in smaller as-deposited grains. However, recrystallization during $CdCl_2$ treatment results in overall comparable grain sizes between different deposition methods [36]. The properties of $CdTe_{1-x}Se_x$ are therefore expected to depend on deposition parameters as well as $CdCl_2$ treatment conditions.

2.1. Crystal Structure

CdTe crystallizes in the cubic zinc blende structure, while CdSe crystallizes in the hexagonal wurzite structure. The two structures are closely related; each Cd^{2+} ion is surrounded by a tetrahedron of four Se^{2-} and/or Te^{2-} ions. In the solid solution $CdTe_{1-x}Se_x$, both the zinc blende and the wurzite structure have been reported [16,34,37–39]. For $0.2 \leq x \leq 0.5$, cubic zinc blende is the low-temperature structure, with a transition to hexagonal wurzite at temperatures above 800 °C. This transition temperature decreases with increasing x, and at $x = 0.6$ the hexagonal wurzite structure is formed at 600 °C [16,37]. With appropriate deposition parameters, mainly dependent on substrate temperature, the entire composition range of $CdTe_{1-x}Se_x$ can be fabricated in the zinc blende structure. In this structure, the lattice constant a decreases with increasing x, following Vegard's law, due to the smaller size of Se^{2-} compared to Te^{2-} [7,33,40,41]. The wurzite structure can occur at room temperature for $x = 0.3$ and higher, sometimes mixed with the zinc blende structure [34,38,39]. In solar cell applications,

the zinc blende structure is desired, as it is photoactive, i.e., it can convert light into photovoltaic current, while the wurzite structure is not photoactive [16].

2.2. Optical Properties

CdTe$_{1-x}$Se$_x$ has a direct band gap with a pronounced bowing behavior. Figure 1 shows reported band gaps of CdTe$_{1-x}$Se$_x$ thin films measured with different methods, as well as one band gap bowing derived from first-principles DFT calculations, all showing a similar bowing behavior trend. The bowing parameter b can be extracted from experimental data with a second-degree polynomial fit. The band gap of any composition x can then be calculated using Equation (1) [42]:

$$E_G(x) = x \cdot E_G^{CdSe} + (1 - x) \cdot E_G^{CdTe} - b \cdot x \cdot (1 - x) \tag{1}$$

Band gap bowing parameters from bulk and thin-film CdTe$_{1-x}$Se$_x$, fabricated by different methods and using different measurement techniques, are listed in Table 1. The published bowing parameter values cover a range of 0.56–0.97, and they all agree on the composition of the band gap minimum at $0.3 \leq x \leq 0.4$, independent of fabrication method. The bowing only marginally depends on the crystal structure [39]. The band gap determination using photoluminescence and cathodoluminescence seem to yield bowing parameters slightly higher than transmittance/reflectance measurements, but they are still in good agreement [31].

Theoretical calculations using different methods are also shown in Table 1, and they seem to be in good agreement with experimental data [42–44]. The band gap minima in all experiments and calculations are around 1.4 eV, confirming that CdTe$_{1-x}$Se$_x$ is a good candidate for band-gap engineering in CdTe solar cells for the purpose of increasing J_{SC}.

In CdTe$_{1-x}$Se$_x$, the valence band edge is dominated by Se and Te p-orbitals, and the conduction band edge is dominated by Cd s- and p-states. Therefore, the anion substitution would be expected to primarily affect the valence band edge [43,45]. However, first-principles calculations show that the bowing of the band gap is caused by the bowing of both band edges due to strong intra-band coupling in both the valence and the conduction band [44].

The refractive index of CdTe$_{1-x}$Se$_x$ is almost constant over a large range of wavelengths, as well as with changes in composition and film thickness. Use of a CdTe$_{1-x}$Se$_x$ layer is therefore not expected to change the overall reflectance of a solar cell, and the introduction of a CdTe$_{1-x}$Se$_x$ gradient does not introduce a gradient in the refractive index [7,25,32].

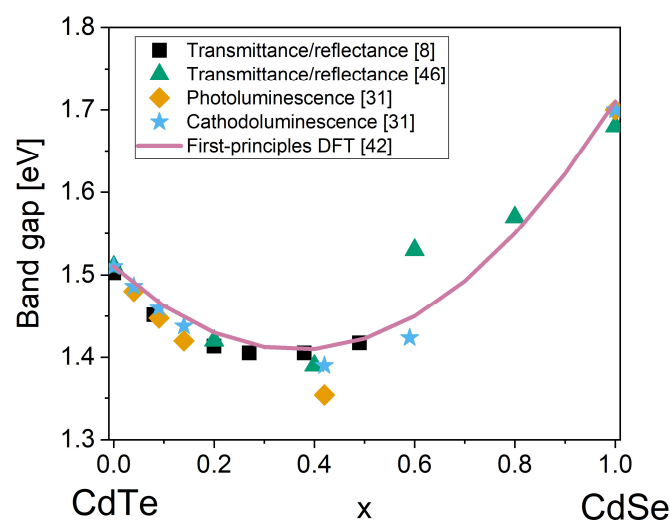**Figure 1.** Band gap bowing of CdTe$_{1-x}$Se$_x$ measured by different methods [8,31,46] and calculated from first-principles DFT [42].

Table 1. Band gap bowing parameters of layers and powders synthesized with different methods.

Source	Deposition	Band Gap Determination	Crystal Structure	x Range	Bowing Parameter	x of Band Gap Minimum	Band Gap Minimum
[39]	Sintering of mixed CdTe and CdSe powders	Transmittance/reflectance	zinc blende	0–0.6	0.74	0.35	1.38
[39]	Sintering of mixed CdTe and CdSe powders	Transmittance/reflectance	wurzite	0.4–1	0.68	0.33	1.4
[8]	Co-evaporation of CdTe and CdSe	Transmittance/reflectance	zinc blende	0–0.5	0.78	0.37	1.39
[7]	Electron-beam evaporation	Transmittance/reflectance	zinc blende	0–1	0.567	0.37	1.44
[46]	Thermal evaporation of mixed CdTe and CdSe powders	Transmittance/reflectance	zinc blende	0–1	0.571	0.35	1.44
[31]	Molecular beam epitaxy on Si	Photoluminescence	zinc blende	0–1	0.97	0.40	1.35
[31]	Molecular beam epitaxy on Si	Cathodoluminescence	zinc blende	0–1	0.82	0.38	1.39
[42]	–	First-principles DFT calculations	zinc blende	0–1	0.75	0.40	1.41
[43]	–	sp^3s^* tight-binding method calculations	zinc blende	0–1	0.904	0.39	1.37
[44]	–	First-principle hybrid-functional calculations	zinc blende	0–1	0.725	0.39	1.43

2.3. Electronic Properties

The electronic properties of $CdTe_{1-x}Se_x$ have not been studied extensively. As-deposited $CdTe_{1-x}Se_x$ is an n-type semiconductor with carrier densities between 10^{13} cm^{-3} (CdTe) and 10^{18} cm^{-3} (CdSe) [40]. The Hall mobility increases by less than an order of magnitude between CdTe and CdSe. Both carrier density and mobility are dependent on deposition temperature, with higher values at higher deposition temperatures due to increased grain size and possibly a reduction in structural defects [26,40]. In solar cell processing, the $CdTe_{1-x}Se_x$ layer is subjected to a $CdCl_2$ treatment, during which it recrystallizes. In CdTe, the recrystallization results in larger grains, reduced structural defects, and reduced recombination [18,47]. A similar effect is expected for $CdTe_{1-x}Se_x$. In absorbers consisting of a $CdTe_{1-x}Se_x$ layer in front of CdTe, recrystallization during $CdCl_2$ treatment has been shown to be responsible for a reduction in stacking faults, combined with interdiffusion of the $CdTe_{1-x}Se_x$ and CdTe layers [19,28].

In solar cells that use $CdTe_{1-x}Se_x$ as part of the absorber layer, dopants are generally added to the whole $CdTe_{1-x}Se_x$/CdTe stack and permeate the $CdTe_{1-x}Se_x$ layer via diffusion. A commonly used extrinsic dopant is copper, which forms deep acceptors as Cu on a Cd site (Cu_{Cd}) [48,49]. First-principles calculations indicate that the formation energy of this acceptor defect exhibits a bowing, with lower formation energies in the $CdTe_{1-x}Se_x$ solid solution than in either parent compound [44]. In the mixed alloy, the bonding Te orbitals are partially replaced with Se orbitals, which have a lower energy. The electronic effects of this change in bonding orbitals are one reason for the bowing behavior. Another reason is the smaller lattice constant with increasing x leading to reduced compressive strain when Cd is replaced by the much smaller Cu [44]. The reduced formation energy indicates better dopability of $CdTe_{1-x}Se_x$ with copper compared to CdTe. However, Hall effect measurements of $CdTe_{1-x}Se_x$ with $0 \leq x \leq 0.2$, deposited by high-vacuum evaporation and subjected to a $CdCl_2$ treatment, revealed that the achievable doping concentration is lower in Se-containing samples, with more than an order of magnitude difference between CdTe and $x = 0.2$ [8]. A possible explanation is that compensating donors, such as copper on interstitial sites (Cu_i), are formed as well, and that the formation energy of

these defects is also dependent on x. If the electronic and/or structural effects of $CdTe_{1-x}Se_x$ alloying facilitate the formation of compensating donors more than the formation of acceptor defects, the result is a limit to the achievable hole density [8,49,50].

The photoluminescence decay of $CdTe_{1-x}Se_x$ measured by time-resolved photoluminescence (TRPL) is generally dominated by surface recombination, resulting in short apparent lifetimes [23,51]. In order to get a reliable measure for the bulk minority carrier lifetime, the surface has to be passivated, e.g., using Al_2O_3, which provides field-effect passivation [52]. Another approach is two-photon excitation (2PE) TRPL, which allows for lifetime measurements at a selected depth of the absorber [51,53]. In $CdTe_{1-x}Se_x$ layers ($x = 0.2$, deposited by close space sublimation and subjected to $CdCl_2$ treatment) with both surfaces passivated by sputtered Al_2O_3, lifetimes of up to 430 ns were measured, an order of magnitude higher than lifetimes in similarly passivated CdTe [23]. The reason seems to be that Se passivates a deep defect in the bulk of the absorber, even at low concentrations [19]. This is also correlated with longer diffusion length in material with higher x [13,19]. Two-photon excitation TRPL measurements performed on an interdiffused $CdTe_{1-x}Se_x$/CdTe absorber (close space sublimation, $CdCl_2$ treated, resulting maximum Se content $x \approx 0.16$) have shown lifetimes of around an order of magnitude higher in the Se-rich front layer compared to the CdTe back layer. This lifetime difference within a single absorber was linked to reduced recombination at the grain boundaries in the Se-containing region [51,53]. Se therefore, at least up to $x \approx 0.2$, seems to provide both passivation of a bulk defect and of the grain boundaries, resulting in an overall increased lifetime. Further studies are needed to accurately determine the lifetime dependence with x, and to determine the steepness of the lifetime gradient in an interdiffused $CdTe_{1-x}Se_x$/CdTe absorber.

The various deposition methods used for CdSe or $CdTe_{1-x}Se_x$ apply a variety of substrate temperatures and deposition rates. We expect that the reported properties of $CdTe_{1-x}Se_x$ may depend on deposition method as well as on the parameters of the $CdCl_2$ treatment, but further investigations are needed to determine the extent.

3. $CdTe_{1-x}Se_x$ in Solar Cells

In recent years, $CdTe_{1-x}Se_x$ has been used as a layer at the front of a predominantly CdTe absorber layer (see Figure 2), either deposited as CdSe or as $CdTe_{1-x}Se_x$, which interdiffuse with CdTe during $CdCl_2$ treatment to form a continuous composition gradient. This results in an absorber layer with a low band gap, increasing the J_{SC}, and it allows for a reduction in CdS thickness, both in superstrate and substrate configuration. As a further step, Munshi et al. [15] replaced the CdS with MgZnO for the highest device efficiencies. Schematics of the different device configurations in which $CdTe_{1-x}Se_x$ layers have been used are shown in Figure 2, from CdS/$CdTe_{1-x}Se_x$/CdTe (Figure 2b), to $CdTe_{1-x}Se_x$/CdTe (Figure 2c), to MgZnO/$CdTe_{1-x}Se_x$/CdTe (Figure 2d). As an alternative to the conventional superstrate configuration, a device in substrate configuration (Figure 2e) is discussed as well.
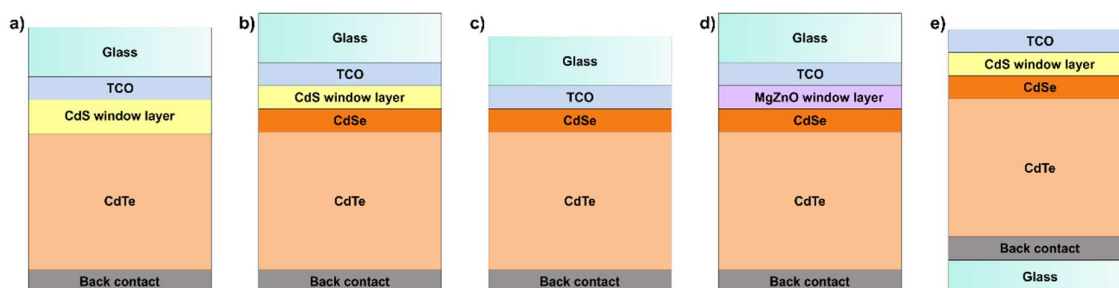

Figure 2. Schematics of deposited layers for solar cells (intermixing not depicted, thicknesses not to scale) for (**a**) a conventional CdTe device, (**b**) a device with a CdSe layer between CdTe and CdS [20]; (**c**) a device with CdSe replacing CdS [14,16]; (**d**) a device with MgZnO and CdSe replacing CdS [15]; and (**e**) a device in substrate configuration with a CdSe layer between CdTe and CdS [8].

The best reported devices for each of the different structures in Figure 2 are listed in Table 2, as well as the CdTe$_{1-x}$Se$_x$-containing record device by First Solar. By removing the CdS layer, a small increase in J_{SC} and FF has been shown, due to reduced parasitic absorption of CdS, at the cost of some losses in V_{OC}, due to interface recombination at the TCO/CdTe$_{1-x}$Se$_x$ interface [20]. With a MgZnO window layer, all device parameters could be improved: high J_{SC} due to the absence of parasitic absorption in the window layer, and high V_{OC} and FF due to a good band alignment between MgZnO and CdTe$_{1-x}$Se$_x$, resulting in a power conversion efficiency of 19.1% [15]. For the substrate configuration device, while the FF is comparable to superstrate devices, the V_{OC} and J_{SC} are lower. The loss in V_{OC} may be due to interface recombination at the CdS/CdTe$_{1-x}$Se$_x$ interface; the loss in J_{SC} due to parasitic absorption in the remaining CdS layer [8]. The world record device from First Solar surpasses all other devices in terms of V_{OC} and J_{SC}, and only the MgZnO/CdTe$_{1-x}$Se$_x$ device can exceed its FF. The exact structure and therefore the reasons for this outstanding performance are not public knowledge, but the high J_{SC} and V_{OC} indicate the use of MgZnO or a similar window layer [3,9,10].

Table 2. *J-V* parameters of the best CdTe$_{1-x}$Se$_x$-containing devices for each configuration shown in Figure 2.

Source	Device Structure	V_{OC} [mV]	J_{SC} [mA/cm^2]	FF [%]	Efficiency [%]
Paudel and Yan [20]	Figure 2b	806	27.2	64.1	14.1
Paudel and Yan [20]	Figure 2c	771	27.5	69.4	14.7
Munshi et al. [15]	Figure 2d	854	28.4	79.1	19.1
Lingg et al. [8]	Figure 2e	710	25.6	67	12.2
First Solar [3,9,10]	unknown	887.2	31.69	78.5	22.1

In the following section, we will first discuss the deposition methods used to form a CdTe$_{1-x}$Se$_x$/CdTe solar cell absorber, and in subsequent subsections we will discuss the details of how CdTe$_{1-x}$Se$_x$ has been used to improve performance in devices with different configurations.

3.1. Formation of a CdTe$_{1-x}$Se$_x$ Layer during Device Processing

Different deposition methods have been used to form a CdTe$_{1-x}$Se$_x$ layer. In conventional superstrate configuration, CdSe can be deposited by high-vacuum evaporation [27], magnetron sputtering [14,16,47], or pulsed laser deposition [54], with CdTe$_{1-x}$Se$_x$ formation during CdCl$_2$ treatment. An alternative is close-space sublimation (CSS) of a CdTe$_{1-x}$Se$_x$ layer [15,19,29]. The CdSe or CdTe$_{1-x}$Se$_x$ layer is followed by deposition of CdTe, CdCl$_2$ and doping treatments, and back contact deposition.

For devices in substrate configuration, a CdSe layer is deposited onto CdTe, followed by CdCl$_2$ and doping treatments and window layer/front contact deposition (see Figure 2e) [8].

In all of these device structures, the absorber and window layer are recrystallized and the CdSe/CdTe$_{1-x}$Se$_x$ interdiffuse with the CdTe during CdCl$_2$ treatment. In an as-deposited CdTe$_{1-x}$Se$_x$ and CdTe absorber, a large number of small grains towards the front (CdTe$_{1-x}$Se$_x$) and increasing grain size towards the back are observed, but after the CdCl$_2$ treatment, the grains are uniform in size and no distinct boundary is visible between CdTe$_{1-x}$Se$_x$ and CdTe [28]. Scanning transmission electron microscopy (STEM)/energy-dispersive x-ray spectroscopy (EDS) mapping reveals interdiffusion of CdTe$_{1-x}$Se$_x$ and CdTe, with Se diffusing more than a μm into the CdTe layer [15,28]. Secondary ion mass spectrometry (SIMS) reveals accumulation of Se at grain boundaries in the CdTe layer, and a relative loss of Se at grain boundaries in the CdTe$_{1-x}$Se$_x$ layer, which is a strong indication for a combination of fast diffusion of Se along the grain boundaries and slow diffusion into the grains [19].

Any photons with energies above the CdTe band gap ($\geq$1.5 eV) are absorbed in the CdTe$_{1-x}$Se$_x$ layer or in the CdTe absorber underneath. CdTe$_{1-x}$Se$_x$ has a lower band gap than CdTe (down to 1.4 eV), and it therefore absorbs photons that cannot be absorbed by CdTe. To maximize J_{SC} gain, the CdTe$_{1-x}$Se$_x$ layer has to be sufficiently thick to absorb the majority of these photons with energies

below the CdTe band gap. If it is formed from CdSe, the composition of the CdTe$_{1-x}$Se$_x$ layer after interdiffusion depends on the thickness of the deposited CdSe layer as well as on the annealing conditions. Yan et al. found that for CdSe layers up to 100 nm thick, the interdiffusion is sufficient to result in a completely photoactive zinc blende absorber with compositions of $x \leq 0.65$. For thicker layers, a non-photoactive wurzite layer with $x > 0.65$ remains at the front of the absorber, which is undesirable because of parasitic absorption. With this method, it is difficult to achieve a thick photoactive layer for full absorption without formation of a non-photoactive layer [16,20,47]. Forming the CdTe$_{1-x}$Se$_x$ layer by depositing CdTe$_{1-x}$Se$_x$ with $x \leq 0.65$ instead of CdSe allows for a higher overall Se content in the absorber because the risk of forming a non-photoactive wurzite layer is minimized, and thick photoactive low-band gap layers can be formed [15].

The interdiffusion of CdTe$_{1-x}$Se$_x$ and CdTe creates a compositional gradient, which is expected to be correlated to the gradient in the material properties of CdTe$_{1-x}$Se$_x$, such as band gap, lattice constant, charge carrier concentration, and minority carrier lifetime. In particular, Fiducia et al. [19] reported gradients in both band gap and diffusion length (determined from cathodoluminescence measurements) that are directly correlated with the Se concentration gradient in a CdTe$_{1-x}$Se$_x$/CdTe device.

3.2. Overview of Device Performances with CdTe$_{1-x}$Se$_x$

Different research groups have had varying success in improving device performance using CdSe. Published device parameters are listed in Table 3, where the parameters are compared with reference devices without CdSe. Generally, the J_{SC} could be improved by the reduced band gap and by reducing or removing the CdS layer. V_{OC} losses are partially due to the reduced band gap. Further V_{OC} losses together with fill factor losses have been mostly attributed to interface recombination, but they were not further investigated. The highest V_{OC} was achieved by use of a MgZnO window layer instead of CdS. The deposition methods are also listed as they may have an influence on the material properties and device performance. The different approaches and results are discussed in the following subsections.

Table 3. *J-V* parameters of devices containing CdSe compared with non-CdSe devices. Deposition methods are abbreviated as RFS (radio frequency sputtering), CSS (close space sublimation), and HVE (high vacuum evaporation).

Source	Device Structure	V_{OC} [mV]	J_{SC} [mA/cm^2]	FF [%]	Efficiency [%]
Poplawsky et al. [16]	CdSe (100 nm, RFS)/CdTe (CSS)	770	27	60.2	12.6
	CdS (130 nm, RFS)/CdTe (CSS)	810	23.8	75.4	14.5
	difference with CdSe	−40	+3.2	−15.2	−1.9
Mia et al. [14]	CdSe (100 nm, RFS)/CdTe (CSS)	690	26.9	64.8	12.1
	CdS (140 nm, RFS)/CdTe (CSS)	847	24.7	70	14.6
	difference with CdSe	−157	+2.2	−5.2	−2.5
Paudel and Yan [20]	CdSe (100 nm RFS)/CdTe (CSS)	771	27.5	69.4	14.7
	CdS (15 nm, RFS)/CdSe (100 nm, RFS)/CdTe (CSS)	806	27.2	64.1	14.1
	CdS (130 nm, RFS)/CdTe (CSS)	811	24.2	75.5	14.8
	difference only CdSe	−40	+3.3	−6.1	−0.1
	difference mixed CdS/CdSe	−5	+3	−11.4	−0.7
pLingg et al. [8]	CdS (30 nm)/CdSe (60 nm)/CdTe (all HVE, substrate config.)	710	25.6	67	12.2
	CdS (120 nm)/CdTe (all HVE, substrate config.)	830	18.5	69.4	10.5
	difference with CdSe	−120	+7.1	−2.4	+1.7
Munshi et al. [15]	MgZnO (RFS)/CdTe$_{0.8}$Se$_{0.2}$ (800 nm, CSS)/CdTe (CSS)	854	28.4	79.1	19.1
	MgZnO (RFS)/CdTe (CSS)	860	26.3	78.9	17.9
	difference with CdSe	−6	+2.1	+0.2	+1.2
First Solar [3,9,10]	CdTe$_{1-x}$Se$_x$/CdTe *	887.2	31.69	78.5	22.1
	CdS/CdTe *	875.9	30.25	79.4	21
	difference with CdSe	+11.3	+1.44	−0.9	+1.1

* The exact device structures and methods of deposition used in the First Solar record devices are not public knowledge.

3.3. CdSe/CdTe Devices without a Window Layer

The performance of devices where the CdS window layer is completely substituted by a CdSe layer (Figure 2c) depends strongly on the thickness of the CdSe layer. Up to 100 nm thick CdSe layers completely interdiffuse with the CdTe during CdCl$_2$ treatment, forming photoactive zinc blende CdTe$_{1-x}$Se$_x$. This results in increased J_{SC} compared to CdS/CdTe devices (see Figure 3) on the one hand because of increased absorption in the long-wavelength region due to a reduced band gap of the absorber, and on the other hand because the absorbing CdS layer is eliminated (see Figure 4). The overall efficiency however is still reduced because of losses in V_{OC} and FF.
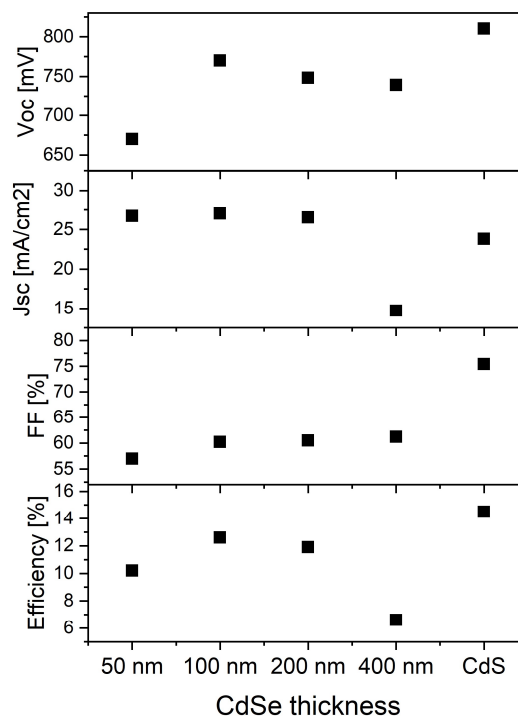

Figure 3. Performance of CdSe/CdTe solar cells with different CdSe thicknesses (values taken from Poplawsky et al. [16]).
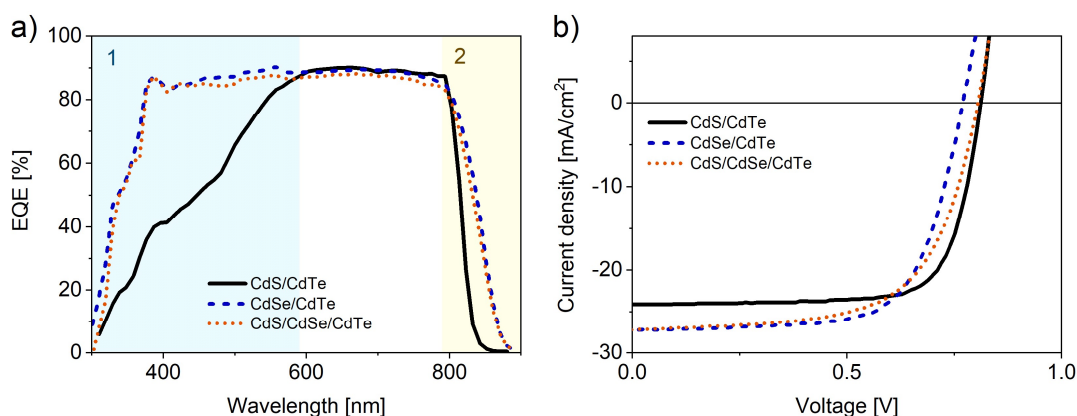

Figure 4. External quantum efficiency (EQE) (**a**) and *J-V* (**b**) curves of solar cells with different window layers (adapted from [20]).

With thicker CdSe layers, the interdiffusion is not complete, and the J_{SC} is reduced due to parasitic absorption in residual non-photoactive wurzite CdTe$_{1-x}$Se$_x$ with high Se content ($x > 0.65$). With optimized CdSe thickness, the J_{SC} can be increased by more than 3 mA/cm^2, however, this is not

sufficient to offset the losses in V_{OC}, which are attributed to high interface recombination at the direct contact between $CdTe_{1-x}Se_x$ and TCO [16,20].

The TCO used in CdTe and $CdTe_{1-x}Se_x$/CdTe devices is usually a bilayer of a low-resistivity material, such as SnO_2:F (FTO), and a high-resistivity material, such as SnO_2. The highly resistive transparent (HRT) layer is used to prevent direct contact between the absorber and the FTO in the case of incomplete CdS coverage [55]. Baines et al. [12] investigated different oxides as HRT layers for $CdTe_{1-x}Se_x$ absorbers and found SnO_2 to be the best. It reduces V_{OC} losses that occur from direct contact of $CdTe_{1-x}Se_x$ with FTO, but the interface recombination is still higher than with a CdS layer [12,20]. In fact, the devices listed in Table 3 all use a SnO_2 HRT layer.

With electron-beam induced current (EBIC) measurements the position of the junction can be determined: for up to 100 nm CdSe, the junction is located at the $CdTe_{1-x}Se_x$/TCO interface. This reveals that the $CdTe_{1-x}Se_x$ does not act as a window layer, but as part of the p-side of the junction. For thicker CdSe layers, the junction is shifted into the $CdTe_{1-x}Se_x$ layer, to the interface between photoactive and non-photoactive $CdTe_{1-x}Se_x$ [16]. The V_{OC} and J_{SC} decrease for thicker layers, confirming that the presence of the non-photoactive wurzite $CdTe_{1-x}Se_x$ is not beneficial for the device performance. Deposition methods and parameters therefore have to be chosen to minimize the formation of non-photoactive $CdTe_{1-x}Se_x$.

3.4. CdSe/CdTe Devices with a CdS Window Layer

With a combined CdS/CdSe window layer (Figure 2b), device performance can be increased by combining the upsides of both layers while minimizing the drawbacks (see Table 3). By reducing the CdS thickness from 130 nm in a CdS/CdTe device to 15 nm in a CdS/CdSe/CdTe device, the parasitic absorption in the short-wavelength region is minimized (region 1 in Figure 4a) and the J_{SC} is increased. Further J_{SC} increase is due to a shift in band gap with $CdTe_{1-x}Se_x$ (region 2 in Figure 4a). The J_{SC} is therefore very similar to a CdSe/CdTe device, while the V_{OC} is improved with the CdS layer in between the $CdTe_{1-x}Se_x$ and the TCO, which reduces the interface recombination (see Figure 4b) [20,54].

A CdS/CdSe/CdTe structure also works in substrate configuration solar cells (Figure 2e). Substrate configuration CdTe solar cells require a thick CdS layer in order to mitigate the formation of pinholes. With a $CdTe_{1-x}Se_x$ layer between CdTe and CdS, the CdS layer thickness can be reduced from 120 to 30 nm with only small losses in V_{OC} and with a 7.1 mA/cm^2 increase in J_{SC} due to the reduction in CdS thickness and the reduction in band gap, resulting in an overall improvement in efficiency (see Table 3) [8].

3.5. CdTe$_{1-x}$Se$_x$/CdTe Devices with a MgZnO Window Layer

Recent high-efficiency CdTe devices have been achieved by replacing the CdS window layer with MgZnO (see Table 3) [15,22]. MgZnO has a band gap of 3.7 eV, higher than CdS, thereby reducing parasitic absorption, and it has a better band alignment with CdTe than TCO/CdS, reducing interface recombination and allowing for a higher V_{OC} [21,22]. However, introduction of a MgZnO window layer into a device structure can be problematic. The MgZnO/CdTe interface is sensitive to barriers originating from oxides, e.g., MgO, that can be formed during deposition. To obtain high-efficiency MgZnO/CdTe devices, deposition parameters, such as temperature and oxygen partial pressure during deposition, and $CdCl_2$ treatment, have to be carefully optimized [56].

Further improvement was achieved by using a $CdTe_{1-x}Se_x$ layer at the front of the CdTe absorber. With an 800 nm thick $CdTe_{1-x}Se_x$ layer in front of a CdTe absorber, Munshi et al. showed an improvement in device efficiency from 17.9% for a MgZnO/CdTe device to 19.1% in a MgZnO/$CdTe_{1-x}Se_x$/CdTe device (see Table 3) [15]. They improved the J_{SC} by 2.1 mA/cm^2 while retaining the high V_{OC} (see Figure 5a). As the device contains no CdS, the EQE in the short-wavelength region is improved (region 1 in Figure 5a).
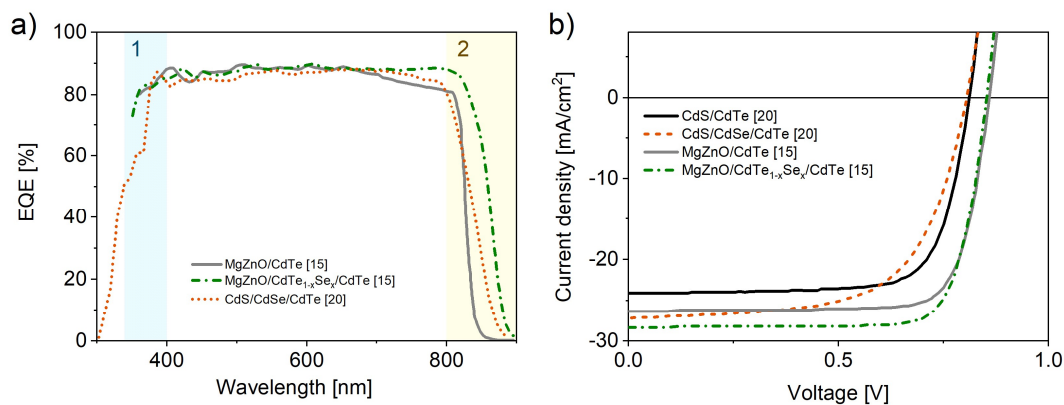
Figure 5. EQE (**a**) and *J-V* (**b**) curves of MgZnO/CdTe and MgZnO/CdTe$_{1-x}$Se$_x$/CdTe devices (adapted from [15]) compared with a CdS/CdSe/CdTe device (adapted from [20]).

The benefit of depositing CdTe$_{1-x}$Se$_x$ instead of CdSe in front of CdTe is the low possibility that non-photoactive wurzite CdTe$_{1-x}$Se$_x$ is formed. As a consequence, higher amounts of Se can be introduced to the device for better fine-tuning of the band gap gradient [29]. This results in a thicker photoactive low-band gap CdTe$_{1-x}$Se$_x$ layer in the finished device. The low-band gap region appears sufficiently thick to absorb most photons with energies below the band gap of CdTe, down to about 1.42 eV, as evidenced by the shift in absorption edge in the EQE curve in region 2 in Figure 5a. The difference in absorption between the thick photoactive layer achieved with CdTe$_{1-x}$Se$_x$ deposition and the thin photoactive layer achieved with CdSe deposition can be seen in the steepness of the EQE curve in region 2 in Figure 5a. The conclusion can be drawn that for maximized J_{SC} gain from CdTe$_{1-x}$Se$_x$, deposition of a CdTe$_{1-x}$Se$_x$ layer instead of a CdSe layer is necessary.

The high V$_{OC}$ in the MgZnO/CdTe$_{1-x}$Se$_x$/CdTe device was in part attributed to a high lifetime of 22 ns measured by TRPL, four times higher than in the MgZnO/CdTe device, due to improved interface quality between MgZnO and CdTe$_{1-x}$Se$_x$, and also due to the passivation of a recombination center by Se [13,15,19]. The MgZnO/CdTe$_{1-x}$Se$_x$/CdTe device has a much higher V_{OC} than the CdS/CdTe$_{1-x}$Se$_x$/CdTe devices. This indicates that the V_{OC} in these structures is limited by the TCO/CdS/CdTe$_{1-x}$Se$_x$ interfaces, but further investigations into the V$_{OC}$ and FF loss of CdTe$_{1-x}$Se$_x$/CdTe devices is needed to confirm this.

Figure 6 compares the EQE curve of the high-efficiency MgZnO/CdTe$_{1-x}$Se$_x$/CdTe device with the record device from First Solar. The First Solar device uses a CdTe$_{1-x}$Se$_x$ layer and some kind of buffer layer instead of CdS [11]. It has a higher V_{OC} and higher J_{SC} than the MgZnO/CdTe$_{1-x}$Se$_x$/CdTe device (see Table 3) [3,11]. The increase in J_{SC} is primarily due to a very good absorption at high wavelengths (region 2 in Figure 6). The very straight absorption edge indicates the presence of a sufficiently thick CdTe$_{1-x}$Se$_x$ layer with a band gap of 1.4 eV for complete absorption of photons in this region. Some further improvement of J_{SC} is achieved by an overall higher EQE, probably due to an antireflection coating. In the short-wavelength region (region 1 in Figure 6), the curves are very similar. This is an indication that First Solar must have used MgZnO or a similar material as a buffer layer, eliminating the influence of parasitic absorption. The increase in V$_{OC}$ might be due to better interface engineering and therefore reduced recombination, but without more information on the First Solar device structure no conclusions can be drawn.
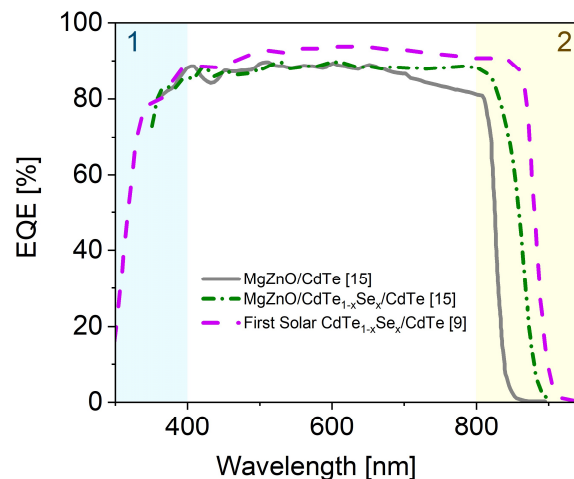
Figure 6. EQE curves of Munshi et al. (adapted from [15]) and the First Solar record device (adapted from [9]).

4. Conclusions

CdTe$_{1-x}$Se$_x$ has been successfully introduced into CdTe devices by several different groups. It has been shown that a band gap gradient can be achieved by several different techniques and deposition methods. For better control and a higher limit to the amount of Se put into the devices, use of a CdTe$_{1-x}$Se$_x$ layer is preferable to a CdSe layer in order to avoid formation of non-photoactive wurzite CdTeSe. In devices with a CdTe$_{1-x}$Se$_x$ layer at the front of the CdTe absorber, the reduced band gap and possibility of reduced CdS window layer thickness result in increased short-circuit current. The open circuit voltage can be maintained at the level of CdTe devices due to Se passivating a recombination center in the absorber. The best reported devices use a MgZnO window layer instead of CdS, which provides a better band alignment with the absorber and eliminates parasitic absorption from the window layer.

Conflicts of Interest: The authors declare no conflict of interest.

References

1.   Philipps, S.; Warmuth, W. *Photovoltaics Report*; Fraunhofer ISE: Freiburg, Germany, 2019.
2.   First Solar Press Release. *First Solar Achieves Yet another Cell Conversion Efficiency World Record*; First Solar Press Release: Tempe, AZ, USA, 2016.
3.   Green, M.A.; Emery, K.; Hishikawa, Y.; Warta, W.; Dunlop, E.D. Solar cell efficiency tables (version 48). *Prog. Photovolt. Res. Appl.* **2016**, *24*, 905–913. [CrossRef]
4.   Geisthardt, R.M.; Topič, M.; Sites, J.R. Status and potential of CdTe solar-cell efficiency. *IEEE J. Photovolt.* **2015**, *5*, 1217–1221. [CrossRef]
5.   Shockley, W.; Queisser, H.J. Detailed balance limit of efficiency of p-n junction solar cells. *J. Appl. Phys.* **1961**, *32*, 510. [CrossRef]
6.   Rühle, S. Tabulated values of the Shockley–Queisser limit for single junction solar cells. *Sol. Energy* **2016**, *130*, 139–147. [CrossRef]
7.   Islam, R.; Banerjee, H.; Rao, D. Structural and optical properties of CdSe$_x$Te$_{1-x}$ thin films grown by electron beam evaporation. *Thin Solid Films* **1995**, *266*, 215–218. [CrossRef]
8.   Lingg, M.; Spescha, A.; Haass, S.G.; Carron, R.; Buecheler, S.; Tiwari, A.N. Structural and electronic properties of CdTe$_{1-x}$Se$_x$ films and their application in solar cells. *Sci. Technol. Adv. Mater.* **2018**, *19*, 683–692. [CrossRef]
9.   Green, M.A.; Emery, K.; Hishikawa, Y.; Warta, W.; Dunlop, E.D. Solar cell efficiency tables (version 46). *Prog. Photovolt. Res. Appl.* **2015**, *23*, 805–812. [CrossRef]

10. Green, M.A.; Emery, K.; Hishikawa, Y.; Warta, W.; Dunlop, E.D. Solar cell efficiency tables (Version 45). *Prog. Photovolt.* **2015**, *23*, 1–9. [CrossRef]

11. Gang, X.; Gloeckler, M. High Efficiency CdTe Solar Cells and Modules. In Proceedings of the E-MRS Spring Meeting, Strasbourg, France, 18–22 June 2018.

12. Baines, T.; Zoppi, G.; Bowen, L.; Shalvey, T.P.; Mariotti, S.; DuRose, K.; Major, J.D. Incorporation of CdSe layers into CdTe thin film solar cells. *Sol. Energy Mater. Sol. Cells* **2018**, *180*, 196–204. [CrossRef]

13. Fiducia, T.A.M.; Munshi, A.H.; Barth, K.; Proprentner, D.; West, G.; Sampath, W.S.; Walls, J.M. Defect tolerance in As-deposited selenium-alloyed cadmium telluride solar cells. In Proceedings of the 2018 IEEE 7th World Conference on Photovoltaic Energy Conversion (WCPEC) (A Joint Conference of 45th IEEE PVSC, 28th PVSEC & 34th EU PVSEC), Waikoloa Village, HI, USA, 10–15 June 2018; pp. 0127–0130.

14. Mia, M.D.; Swartz, C.H.; Paul, S.; Sohal, S.; Grice, C.R.; Yan, Y.; Holtz, M.; Li, J.V. Electrical and optical characterization of CdTe solar cells with CdS and CdSe buffers—A comparative study. *J. Vac. Sci. Technol. B* **2018**, *36*, 052904. [CrossRef]

15. Munshi, A.H.; Kephart, J.; Abbas, A.; Raguse, J.; Beaudry, J.-N.; Barth, K.; Sites, J.; Walls, J.; Sampath, W. Polycrystalline CdSeTe/CdTe absorber cells with 28 mA/cm^2 short-circuit current. *IEEE J. Photovolt.* **2018**, *8*, 310–314. [CrossRef]

16. Poplawsky, J.D.; Guo, W.; Paudel, N.; Ng, A.; More, K.; Leonard, D.; Yan, Y. Structural and compositional dependence of the CdTe$_x$Se$_{1-x}$ alloy layer photoactivity in CdTe-based solar cells. *Nat. Commun.* **2016**, *7*, 12537.

17. Yang, X.; Liu, B.; Li, B.; Zhang, J.; Li, W.; Wu, L.; Feng, L. Preparation and characterization of pulsed laser deposited a novel CdS/CdSe composite window layer for CdTe thin film solar cell. *Appl. Surf. Sci.* **2016**, *367*, 480–484. [CrossRef]

18. McCandless, B.E.; Moulton, L.V.; Birkmire, R.W. Recrystallization and sulfur diffusion in CdCl$_2$-treated CdTe/CdS thin films. *Prog. Photovolt. Res. Appl.* **1997**, *5*, 249–260. [CrossRef]

19. Fiducia, T.A.M.; Mendis, B.G.; Li, K.; Grovenor, C.R.M.; Munshi, A.H.; Barth, K.; Sampath, W.S.; Wright, L.D.; Abbas, A.; Bowers, J.W.; et al. Understanding the role of selenium in defect passivation for highly efficient selenium-alloyed cadmium telluride solar cells. *Nat. Energy* **2019**, *4*, 504–511. [CrossRef]

20. Paudel, N.R.; Yan, Y. Enhancing the photo-currents of CdTe thin-film solar cells in both short and long wavelength regions. *Appl. Phys. Lett.* **2014**, *105*, 183510. [CrossRef]

21. Kephart, J.; McCamy, J.; Ma, Z.; Ganjoo, A.; Alamgir, F.; Sampath, W. Band alignment of front contact layers for high-efficiency CdTe solar cells. *Sol. Energy Mater. Sol. Cells* **2016**, *157*, 266–275. [CrossRef]

22. Munshi, A.H.; Kephart, J.M.; Abbas, A.; Shimpi, T.M.; Barth, K.L.; Walls, J.M.; Sampath, W.S. Polycrystalline CdTe photovoltaics with efficiency over 18% through improved absorber passivation and current collection. *Sol. Energy Mater. Sol. Cells* **2018**, *176*, 9–18. [CrossRef]

23. Kephart, J.M.; Kindvall, A.; Williams, D.; Kuciauskas, D.; Dippo, P.; Munshi, A.; Sampath, W.S. Sputter-deposited oxides for interface passivation of CdTe photovoltaics. *IEEE J. Photovolt.* **2018**, *8*, 587–593. [CrossRef]

24. Russak, M.A.; Creter, C. Vacuum Evaporated CdSe$_{1-x}$Te$_x$ Thin Films for Electrochemical Photovoltaic Cells. *J. Electrochem. Soc.* **1984**, *131*, 556–562. [CrossRef]

25. El-Nahass, M.; Sallam, M.; Afifi, M.; Zedan, I. Structural and optical properties of polycrystalline CdSe$_x$Te$_{1-x}$ ($0 \leq x \leq 0.4$) thin films. *Mater. Res. Bull.* **2007**, *42*, 371–384. [CrossRef]

26. Uthanna, S.; Reddy, P. Structural and electrical properties of CdSe$_x$Te$_{1-x}$ thin films. *Solid State Commun.* **1983**, *45*, 979–980. [CrossRef]

27. Borah, M.N.; Chaliha, S.; Sarmah, P.; Rahman, A. Electrical and optical properties of thin film (n) CdSe/(p) CdTe heterojunction and its performance as a photovoltaic converter. *J. Optoelectron. Adv. M.* **2008**, *10*, 1333–1339.

28. Munshi, A.H.; Kephart, J.M.; Abbas, A.; Danielson, A.; Gélinas, G.; Beaudry, J.-N.; Barth, K.L.; Walls, J.M.; Sampath, W.S. Effect of CdCl$_2$ passivation treatment on microstructure and performance of CdSeTe/CdTe thin-film photovoltaic devices. *Sol. Energy Mater. Sol. Cells* **2018**, *186*, 259–265. [CrossRef]

29. Swanson, D.E.; Sites, J.R.; Sampath, W.S. Co-sublimation of CdSe$_x$Te$_{1-x}$ layers for CdTe solar cells. *Sol. Energy Mater. Sol. Cells* **2017**, *159*, 389–394. [CrossRef]

30. Amir, F.; Clark, K.; Maldonado, E.; Kirk, W.; Jiang, J.; Ager III, J.; Yu, K.; Walukiewicz, W. Epitaxial growth of CdSe$_x$Te$_{1-x}$ thin films on Si (1 0 0) by molecular beam epitaxy using lattice mismatch graded structures. *J. Cryst. Growth* **2008**, *310*, 1081–1087. [CrossRef]

31. Campo, E.M.; Hierl, T.; Hwang, J.C.; Chen, Y.; Brill, G.; Dhar, N.K. Comparison of cathodoluminescence and photoluminescence of CdSeTe films grown on Si by molecular beam epitaxy. In Proceedings of the SPIE, Denver, CO, USA, 22 October 2004.

32. Muthukumarasamy, N.; Balasundaraprabhu, R.; Jayakumar, S.; Kannan, M.D.; Ramanathaswamy, P. Compositional dependence of optical properties of hot wall deposited CdSe$_x$Te$_{1-x}$ thin films. *Phys. Status Solidi (a)* **2004**, *201*, 2312–2318. [CrossRef]

33. Mangalhara, J.; Agnihotri, O.; Thangaraj, R. Structural, optical and photoluminescence properties of electron beam evaporated CdSe$_{1-x}$Te$_x$ films. *Sol. Energy Mater.* **1989**, *19*, 157–165. [CrossRef]

34. Bouroushian, M.; Loizos, Z.; Spyrellis, N.; Maurin, G. Influence of heat treatment on structure and properties of electrodeposited CdSe of Cd(Te, Se) semiconducting coatings. *Thin Solid Films* **1993**, *229*, 101–106. [CrossRef]

35. Kathalingam, A.; Kim, M.R.; Chae, Y.S.; Rhee, J.K.; Thanikaikarasan, S.; Mahalingam, T. Study on electrodeposited CdSe$_x$Te$_{1-x}$ semiconducting thin films. *J. Alloy. Compd.* **2010**, *505*, 758–761. [CrossRef]

36. McCandless, B.E.; Sites, J.R. *Handbook of Photovoltaic Science and Engineering*; John Wiley & Sons: Hoboken, NJ, USA, 2005; pp. 617–662.

37. Strauss, A.J.; Steininger, J. Phase diagram of the CdTe-CdSe pseudobinary system. *J. Electrochem. Soc.* **1970**, *117*, 1420–1426. [CrossRef]

38. Kumar, L.; Singh, B.P.; Misra, A.; Misra, S.; Sharma, T. Characterization of CdSe$_x$Te$_{1-x}$ sintered films for photovoltaic applications. *Phys. B Condens. Matter* **2005**, *363*, 102–109. [CrossRef]

39. Tai, H.; Nakashima, S.; Hori, S. Optical properties of (CdTe)$_{1-x}$(CdSe)$_x$ and (CdTe)$_{1-x}$(CdS)$_x$ systems. *Phys. Status Solidi (a)* **1975**, *30*, K115–K119. [CrossRef]

40. Russak, M.A. Deposition and characterization of CdSe$_{1-x}$Te$_x$ thin films. *J. Vac. Sci. Technol. A* **1985**, *3*, 433–435. [CrossRef]

41. Sanitarov, V.; Aleksandrova, L.; Kalinkin, I. The ranges of isomorphous substitutions in thin films of CdSe$_x$Te$_{1-x}$ solid solutions. *Thin Solid Films* **1982**, *97*, 205–214. [CrossRef]

42. Wei, S.H.; Zhang, S.; Zunger, A. First-principles calculation of band offsets, optical bowings, and defects in CdS, CdSe, CdTe, and their alloys. *J. Appl. Phys.* **2000**, *87*, 1304–1311. [CrossRef]

43. Tit, N.; Obaidat, I.M.; Alawadhi, H. Origins of bandgap bowing in compound-semiconductor common-cation ternary alloys. *J. Phys. Condens. Matter* **2009**, *21*, 075802. [CrossRef]

44. Yang, J.; Wei, S.-H. First-principles study of the band gap tuning and doping control in CdSe$_x$Te$_{1-x}$ alloy for high efficiency solar cell. *Chinese Phys. B* **2019**, *28*, 086106. [CrossRef]

45. Reshak, A.H.; Kityk, I.; Khenata, R.; Auluck, S. Effect of increasing tellurium content on the electronic and optical properties of cadmium selenide telluride alloys CdSe$_{1-x}$Te$_x$: An ab initio study. *J. Alloy. Compd.* **2011**, *509*, 6737–6750. [CrossRef]

46. Santhosh, T.; Bangera, K.V.; Shivakumar, G. Synthesis and band gap tuning in CdSe$_{1-x}$Te$_x$ thin films for solar cell applications. *Sol. Energy* **2017**, *153*, 343–347. [CrossRef]

47. Paudel, N.R.; Moore, K.L.; Yan, Y.; Poplawsky, J.D. Current enhancement of CdTe-based solar cells. *IEEE J. Photovolt.* **2015**, *5*, 1492–1496. [CrossRef]

48. Krasikov, D.; Knizhnik, A.; Potapkin, B.; Selezneva, S.; Sommerer, T. First-principles-based analysis of the influence of Cu on CdTe electronic properties. *Thin Solid Films* **2013**, *535*, 322–325. [CrossRef]

49. Wei, S.H.; Zhang, S.; Zhang, S.B. Chemical trends of defect formation and doping limit in II-VI semiconductors: The case of CdTe. *Phys. Rev. B* **2002**, *66*, 155211. [CrossRef]

50. Gretener, C.; Wyss, M.; Perrenoud, J.; Kranz, L.; Buecheler, S.; Tiwari, A.N. CdTe thin films doped by Cu and Ag-a comparison in substrate configuration solar cells. In Proceedings of the 2014 IEEE 40th Photovoltaic Specialist Conference (PVSC), Denver, CO, USA, 8–13 June 2014; pp. 3510–3514.

51. Kuciauskas, D.; Kanevce, A.; Burst, J.M.; Duenow, J.N.; Dhere, R.; Albin, D.S.; Levi, D.H.; Ahrenkiel, R.K. Minority carrier lifetime analysis in the bulk of thin-film absorbers using subbandgap (two-photon) excitation. *IEEE J. Photovolt.* **2013**, *3*, 1319–1324. [CrossRef]

52. Kuciauskas, D.; Kephart, J.M.; Moseley, J.; Metzger, W.K.; Sampath, W.S.; Dippo, P. Recombination velocity less than 100 cm/s at polycrystalline Al$_2$O$_3$/CdSeTe interfaces. *Appl. Phys. Lett.* **2018**, *112*, 263901. [CrossRef]

53. Zheng, X.; Kuciauskas, D.; Moseley, J.; Colegrove, E.; Albin, D.S.; Moutinho, H.; Duenow, J.N.; Ablekim, T.; Harvey, S.P.; Ferguson, A.; et al. Recombination and bandgap engineering in CdSeTe/CdTe solar cells. *APL Mater.* **2019**, *7*, 071112. [CrossRef]

54. Yang, X.; Bao, Z.; Luo, R.; Liu, B.; Tang, P.; Li, B.; Zhang, J.; Li, W.; Wu, L.; Feng, L. Preparation and characterization of pulsed laser deposited CdS/CdSe bi-layer films for CdTe solar cell application. *Mater. Sci. Semicond. Process.* **2016**, *48*, 27–32. [CrossRef]

55. Feldman, S.; Mansfield, L.; Ohno, T.; Kaydanov, V.; Beach, J.; Nagle, T. Non-uniformity mitigation in CdTe solar cells: The effects of high-resistance transparent conducting oxide buffer layers. In Proceedings of the Conference Record of the Thirty-first IEEE Photovoltaic Specialists Conference, Lake Buena Vista, FL, USA, 3–7 January 2005; pp. 271–274.

56. Ablekim, T.; Perkins, C.; Zheng, X.; Reich, C.; Swanson, D.; Colegrove, E.; Duenow, J.N.; Albin, D.; Nanayakkara, S.; Reese, M.O.; et al. Tailoring MgZnO/CdSeTe Interfaces for Photovoltaics. *IEEE J. Photovolt.* **2019**, *9*, 888–892. [CrossRef]